Engineered Science
DOI: https://dx.doi.org/10.30919/es1513

Enhancing Seismic Resilience of Soft-Storey Buildings through Optimized Reinforced Concrete Infill Solutions

Lin Htin,[1] Kishor Timsina,[2] Chaitanya Krishna Gadagamma,[1,3] Qudeer Hussain,[4] Ali Ejaz,[5] Panumas Saingam,[6] Wasim Khaliq,[5] Gritsada Sua-iam,[6] Burachat Chatveera,[7] Zabihullah Dalil Shinwari,[8] Kriti Shrestha[9] and Suniti Suparp[10, 11,*]

Abstract

This research experimentally validates and establishes guidelines for optimizing the strengthening of reinforced concrete (RC) infill walls, focusing on local availability, response, price, usability, and difficulty. Two main objectives were pursued: (1) analyzing soft-storey frames using applied element method (AEM)-based numerical optimization to develop an effective strengthening solution, and (2) experimentally verifying the performance of the optimized RC infill wall in strengthening soft-storey buildings. The study found that the strengthening solution significantly enhanced structural performance, with the maximum peak load increasing from 7 kN for the soft-storey frame to 73 kN for the strengthened frame, a tenfold increase. The strengthened frame also dissipated energy five times better than the soft-storey frame, demonstrating superior seismic energy absorption. Substantial displacements at the ground floor were mitigated in the strengthened frame, improving stability and stiffness. The strengthened frame's stiffness was about ten times higher than that of the soft-storey frame, attributed to added curves connecting the columns and beams on the ground floor. Additionally, the strengthened frame's natural frequency was 25.62 Hz, lower than the predicted 30.55 Hz, likely due to construction variations. These results highlight the efficacy of the proposed strengthening method in enhancing the seismic resilience of soft-storey buildings.

Keywords: Soft-storey; Strengthening; Applied element method; Capacity; Natural frequency; Energy dissipation; Sustainable development; Green Infrastructure.
Received: 04 January 2025; Revised: 25 January 2025; Accepted: 28 January 2025.
Article type: Research article.

1. Introduction

Soft-storey irregularity is a kind of vertical irregularity found in buildings. In seismic-prone regions, it is recommended to avoid such irregularities to reduce the risk of structural collisions during significant earthquakes. Building codes typically outline specific limits for both vertical and horizontal irregularities to enhance safety. According to ASCE,[1] a soft-storey condition exists when the stiffness of one storey is less than 70% of the stiffness of the adjacent storey or less than 80% of the average stiffness of the three adjacent stories.

Seismic structural design codes play a crucial role in minimizing the seismic risk of buildings, but their effectiveness depends on proper application during the design process and adequate quality control during construction.[2–5] If these codes are not correctly implemented or if construction oversight is inadequate, it can lead to structurally vulnerable buildings.[6,7] Ensuring satisfactory structural performance during earthquakes requires both high-quality design and construction. Recent earthquakes have demonstrated that these factors, particularly the quality of construction, are closely linked to the overall performance of structures under seismic forces.[8–10]

In multi-storey high-rise buildings, specific structural characteristics can result in weak or soft-storey issues.[11] Increased flexibility of the soft-storey results in greater deflection, higher plastic deformation, and stress

[1] *Structural Engineering, School of Engineering and Technology (SET), Asian Institute of Technology (AIT), Klong Luang, 12120, Thailand*
[2] *Madan Bhandari University of Science and Technology (MBUST), Thaha-09, Chitlang, 33300, Nepal*
[3] *Department of Civil Engineering, Chennai Institute of Technology, Chennai, 600036, India*
[4] *Department of Civil Engineering, Kasem Bundit University, Bangkok, 10250, Thailand*
[5] *National Institute of Transportation, National University of Sciences and Technology (NUST), Islamabad, 44000, Pakistan*
[6] *Department of Civil Engineering, School of Engineering, King Mongkut's Institute of Technology, Ladkrabang, Bangkok, 10520, Thailand*

concentration at the connections above the first storey. Additionally, the columns of the soft-storey channel a significant amount of force from the rapid movement of the floors into a failure mechanism. Therefore, soft-storey buildings require special attention during the research and design stages, as their failure under these conditions is highly likely.[12] To enhance the seismic response of soft-storey buildings, strengthening is necessary and can be achieved through both local and global retrofitting procedures.[13,14]

Various procedures for seismic strengthening have been developed and implemented in practice. According to CEB (1997), these techniques are based on three main objectives: (a) increasing the structure's lateral strength, (b) enhancing the structure's ductility, and (c) improving both the strength and ductility of the structure.[15] Generally, reinforced concrete buildings with soft-storey are strengthened either with global strengthening or local strengthening.[16] Global strengthening involves the addition of buttresses or wing walls,[17] shear walls,[18] infill walls,[19] lateral bracing,[20] or mass reduction.[21] Whereas the local strengthening involves the strengthening of buildings' individual members such as beams, columns, footings, or beam-column joints.[16] Additionally, the strengthening could also be extended to include new footings/piles to enhance the global lateral stability. Nonetheless, these methods aim to enhance the structure's lateral rigidity and strength, thus decreasing the probability of failure during an earthquake.[22]

Although numerous methods exist to address the soft-storey issue, they often do not align with societal needs.[23] The available solutions are rarely implemented due to high costs, limited availability of materials, low usability, or inadequate behavior. This indicates a gap between societal needs and technical solutions for this issue. Given that concrete is a easily available material and RC shear walls provide a higher base shear coefficient than other options, optimizing reinforced concrete (RC) infill shear walls could offer a more practical and feasible solution. This optimized approach could serve as a redesign guideline for existing RC structures with soft-storey issues, balancing usability, affordability, and the necessary performance requirements for life safety.[24]

[7] *Department of Civil Engineering, Faculty of Engineering, Thammasat University (Rangsit Campus), Pathum Thani, 12121, Thailand*

[8] *Faculty of Engineering, Kardan University, Kabul, 1001, Afghanistan*

[9] *Gautam Buddha International Airport, Kathmandu, 44600, Nepal*

[10] *Department of Civil and Environmental Engineering, Faculty of Engineering, Srinakharinwirot University, Nakhonnayok, 26120, Thailand.*

[11] *Center of Excellence in Rail System Technology and Civil Engineering Material Innovation for Sustainable Infrastructure, Strategic Wisdom and Research Institute, Srinakharinwirot University, Bangkok, 10110, Thailand*

**Email:* suniti@g.swu.ac.th (S. Suparp)

There are various optimization methodologies available, and the choice of a suitable method depends primarily on the characteristics of the specific optimization problem. In this work, the optimization problem can be described by three key components. First, it is a non-linear constrained problem. Second, the optimization process must integrate a numerical tool, such as the applied element method (AEM), to implicitly evaluate performance constraints at each iteration. The AEM is capable of tracking the complete structural response from the initial loading stage through to collapse, including the progressive failure of the structure, such as crack initiation, propagation, and distribution.[25] Additionally, the boundary limits of performance constraints must be adjusted dynamically in each iteration based on the variables' values at that stage. Therefore, the optimization scheme should be both iterative and dynamic to accommodate these evolving constraints.[26]

Based on a review of social needs and technical aspects of strengthening solutions, there is a demand for practical and implementable strengthening strategies for addressing the soft-storey issue, particularly through the optimization of RC infill walls that consider local accessibility, behavior, price, serviceability, and difficulty. The numerical analysis conducted by Timsina *et al*.[26] developed an optimized framework for resolving soft-storey issues in RC buildings. However, for these solutions to be viable in real-world applications, experimental verification, along with the development of recommendations or guidelines, is necessary. This work targets to provide experimental validation and establish guides for implementing this strengthening strategy. This shall be achieved through three primary aims: first, analyzing case-study soft-storey frame to derive a strengthening strategy by utilizing numerical optimization with AEM; second, experimentally verifying the effectiveness of the optimized RC infill wall for strengthening soft-storey frames; and third, providing recommendations for field implementation based on the experimental results.

2. Methodology

2.1 Overview of the methodology

This work methodology comprises two main parts, each corresponding to a specific objective: numerical analysis, and experimental testing. The experimental work was conducted at the AIT Structural Engineering Laboratory, where monotonic pushover tests were performed on both soft-storey and strengthened frames. To capture data, accelerometers, laser displacement sensors, and data loggers were installed on the side opposite the actuator. All equipment was thoroughly inspected and calibrated beforehand to target their limits and ensure accurate measurements. Fig. 1 depicts a summary of the approach.

The first part of the approach involves numerical analysis of the case-study experimental frame, utilizing the AEM combined with numerical optimization. This process helps determine optimized parameters for strengthening the frames

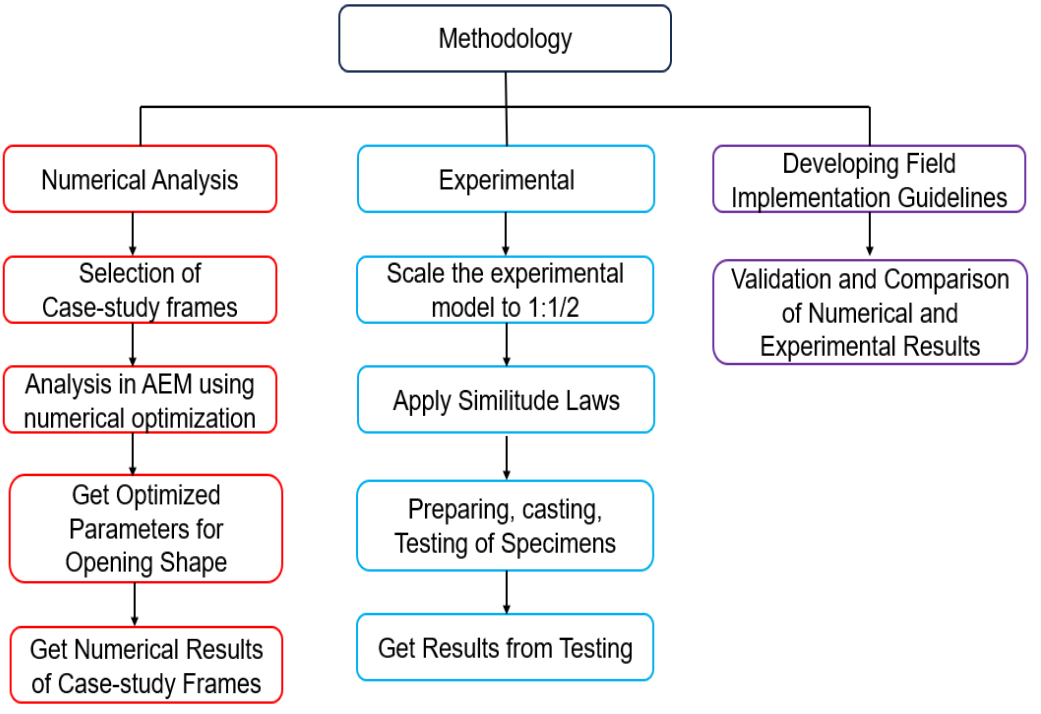

Fig. 1: Overview of the methodology.

with openings. Once the optimal parameters are identified, the experimental frames are scaled down in accordance with similitude requirements, ensuring accurate replication. Following this, the preparation, fabrication, and testing of the specimens are carried out, with pushover tests conducted on both the soft-storey and strengthened frames.

2.2 Details of 2D Frame

The experimental case-study frame is chosen to reflect the situations commonly found in existing frame structures. For this work, a simple 2D frame was chosen to effectively attain both the soft-storey impact and the response of the optimized strengthened strategy. Due to laboratory constraints, the experimental model was halved the size of the sample. To accurately scale the geometric and material characteristics, similitude laws were applied to account for the differences between the sample and its scaled-down version. According to Noor and Boswell,[27] when dealing with structures subjected to static loading, certain considerations can be made: the scaling of the concrete's density can be disregarded, and the inclusion of artificial weights can also be disregarded. According to similitude necessities, when using the same material characteristics and scaling the geometric characteristics by a factor of two, the resulting displacements in the experimental model will also be scaled by a factor of two, while the forces will be scaled by a factor of four.

2.3 Properties of frame

The experimental frames include a soft-storey and a strengthened frame, with strengthening parameters derived from numerical optimization using AEM. The frame has a span of 2 meters center-to-center, with each storey having a height of 1.5 meters. The columns are sized at 125 mm × 125 mm, reinforced with 4 9-mm diameter bars, while the beams also measure 125 mm × 125 mm and are reinforced with 4 9-mm diameter bars. Stirrups and tie bars are made of steel wire with a 6-mm diameter. The concrete used has a compressive strength of 22 MPa and a tensile strength of 2.75 MPa. For the brick material, the compressive strength is 5.15 MPa, and the tensile strength is 0.50 MPa. The main reinforcing bars and the stirrups and ties both have a strength of 380 MPa. Table 1 lists the properties of frames.

Table 1: Properties of experimental frames tested in this study.

Properties/Dimensions	Model
Frame span	2 m
Frame height	1.5 m
Column cross-section	125 × 125
Column bars	Four 9-mm bars
Beam cross-section	125 × 125, 200 × 250
Beam rebar	Four 9-mm bars
Concrete	f_c' = 22.0 MPa, f_t = 2.76 MPa
Brick	f_c'= 5.15 MPa, f_t = 0.50 MPa
Rebar strength	f_y = 390 MPa for 9 mm bars f_y = 390 MPa for 6 mm bars

2.4 Numerical characteristics in AEM

The numerical model is developed utilizing AEM, with discrete elements each sized at 2.50 cm. The coordinates for the columns, beams, and walls are input through text input, and the bases of the columns are assigned as fixed boundary conditions. The model incorporates three material types: concrete, brick, and rebar, each characterized by specific material characteristics, including Young's modulus, tensile

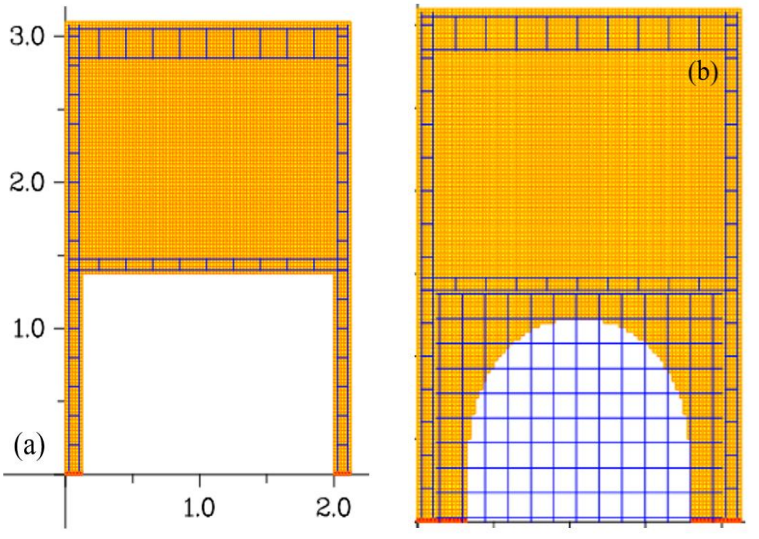

Fig. 2: Numerical views of (a) control and (b) strengthened frames.

capacity, compressive capacity, the quantity of springs that connected elements, density, and the coefficient of restitution. Fig. 2 shows the numerical view of soft-storey (control) and strengthened frames. Table 2 shows numerical properties of frames.

Table 2: Numerical properties of frames.

Properties	Control frame	Strengthened frame
Number of elements	6415	8041
Element size	2.50 cm	2.5 cm
Number of blocks	6.0	5
Boundary elements	10.0	26
Number of bars	56.0	56
Number of springs	125660	158240

2.5 Pushover analysis in AEM

In AEM, pushover loading is applied using a displacement control approach with an increment of 1000 time intervals. The element on the roof is designated as the control element for displacement-controlled loading, and measurements are taken at each interval. The load vs. displacement comparison of control and strengthened frames is illustrated in Fig. 3, which shows the experimental frames scaled down according to similitude requirements. The results indicate that the peak load of the soft-storey frame is significantly lower, whereas the strengthened frame exhibits a much greater peak load. The load capacity of the strengthened frame is nearly ten times higher than that of the soft-storey frame, demonstrating the effectiveness of the strengthening strategy.

2.6 Optimization results for strengthening

The iterations in the numerical optimization process provide various opening parameters for strengthening. Amongst these options, the highest optimized solution was selected depening on a balance of behavior, price, serviceability, and difficulty. Fig. 4 shows the opening parameters for strengthening.

2.7 Trial of flowable concrete for scaled-down frames

Due to the experimental frames being halved of their actual size, challenges such as rebar congestion and difficulty in achieving proper concrete compaction were encountered. To address these issues, micro concrete with good flowability was used in the construction of the frames. Various trial mix proportions were tested, and the results, along with the issues encountered in the lab, are presented in Table 3. Trial No. 1, which did not include any chemical additives, resulted in a concrete paste with poor flowability. Trial No. 2 incorporated a superplasticizer at less than 1.25% of the water content, leading to some bleeding in the concrete. Trials 3 and 4 used silica fume and superplasticizer, with water-to-cement (w/c) ratios of 0.60 and 0.40, respectively. Trial 3 exhibited bleeding, while Trial 4 achieved extremely high compressive strength. Trial 5, which included fly ash to improve workability and had a w/c ratio of 0.6, demonstrated the desired characteristics of a flowable mix. Consequently, Trial 5 was selected for use in the experimental frames. Fig. S1(a) shows the slump test for Trial 5, whereas concrete cylinders cast from Trial 5 are shown in Fig. S1(b).

2.8 Construction of frames

The two footings were initially cast utilizing ready-mix concrete and cured for 7 days. Strain gauges were affixed to the dowel bars used in column lap splicing to monitor strain during lateral push tests. After curing, the footings were transported to the testing site and secured with 14 anchor bolts of 25 mm diameter each. Longitudinal steel bars of the ground floor columns were lap spliced to the dowel bars embedded in the footing, with a lap splice length of approximately 500 mm, and the bars were tied with steel wires. Strain gauges were repositioned as needed, and formwork was prepared for casting concrete. The ground floor columns, first-floor beams, and first-floor slab were cast simultaneously using flowable self-compacting concrete (SCC). After 14 days, the first floor was completed and left to gain strength, followed by brick

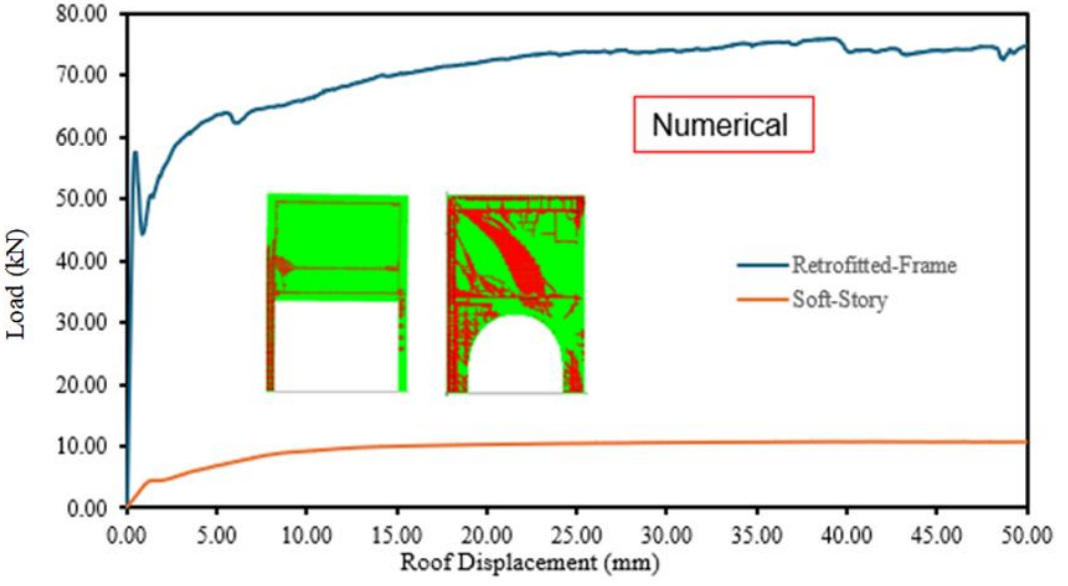

Fig. 3: Load vs. displacement comparison of control and strengthened frames.

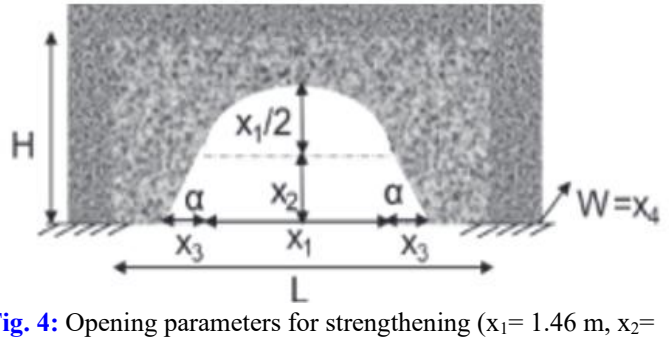

Fig. 4: Opening parameters for strengthening (x_1= 1.46 m, x_2= 0.56 m, x_3= 0.10 m, and x_4= 0.126 m).

walling with scaled-down bricks. For the strengthened frame, construction followed the same steps up to brick walling, as shown in Fig. S2. Strengthening then involved making the column surfaces rough, drilling holes for 9 mm diameter rebars with a rotary hammer drill and inserting the rebars with Sika Adhesive, as shown in Fig. S3. The formwork for both the bottom and top curved portions was constructed and concrete was poured, leaving a 30 mm gap near the top of the curve for proper filling, which was later filled with mortar having a compressive strength of 20 MPa.

2.9 Instrumentation and test setup

Initially, the frame was restricted in the out-of-plane bending utilizing roller frames to inhibit rotation, with the rollers positioned at the top beam as illustrated in Fig. S4. Strain gauges were attached at critical locations on the rebars of the columns and beams. Specifically, 2 strain gauges were utilized on the anchorage rebars for the columns, 8 on the ground floor columns, 5 on the first-floor beam, eight on the first-floor columns, and none on the top beam, totaling 23 strain gauges for the soft-storey frame, as illustrated in Fig. 5. An ambient vibration test was performed to find the natural frequency of the frames, using accelerometers placed on each footing, the first-floor slab, and the top of the frame, with a sampling rate

Table 3: Trial mix proportions for self-compacting concrete (SCC).

Number	ID	Cement (kg/m^3)	Fine aggregates (kg/m^3)	Course aggregates (kg/m^3)	Water (kg/m^3)	S.P (%)	w/c ratio	Issues
1	TR1	350	877	768	240	-	0.67	No flowability
2	TR2	400	877	768	240	<<1.25	0.53	bleeding
Sr. No	Mix	Cement (kg/m^3)	Silica fume (kg/m^3)	Fine aggregates (kg/m^3)	Course aggregates (kg/m^3)	Water (kg/m^3)	S.P (%)	w/c ratio
3	TR3	370	30	877	768	240	<<1.25	0.6 (Bleeding)
4	TR4	370	30	877	768	160	<<1.25	0.4 (Very high strength)
Sr. No	Mix	Cement (kg/m^3)	Fly ash (kg/m^3)	Fine aggregates (kg/m^3)	Course aggregates (kg/m^3)	Water (kg/m^3)	S.P (%)	w/c ratio
5	TR5	340	60	877	768	240	-	0.6

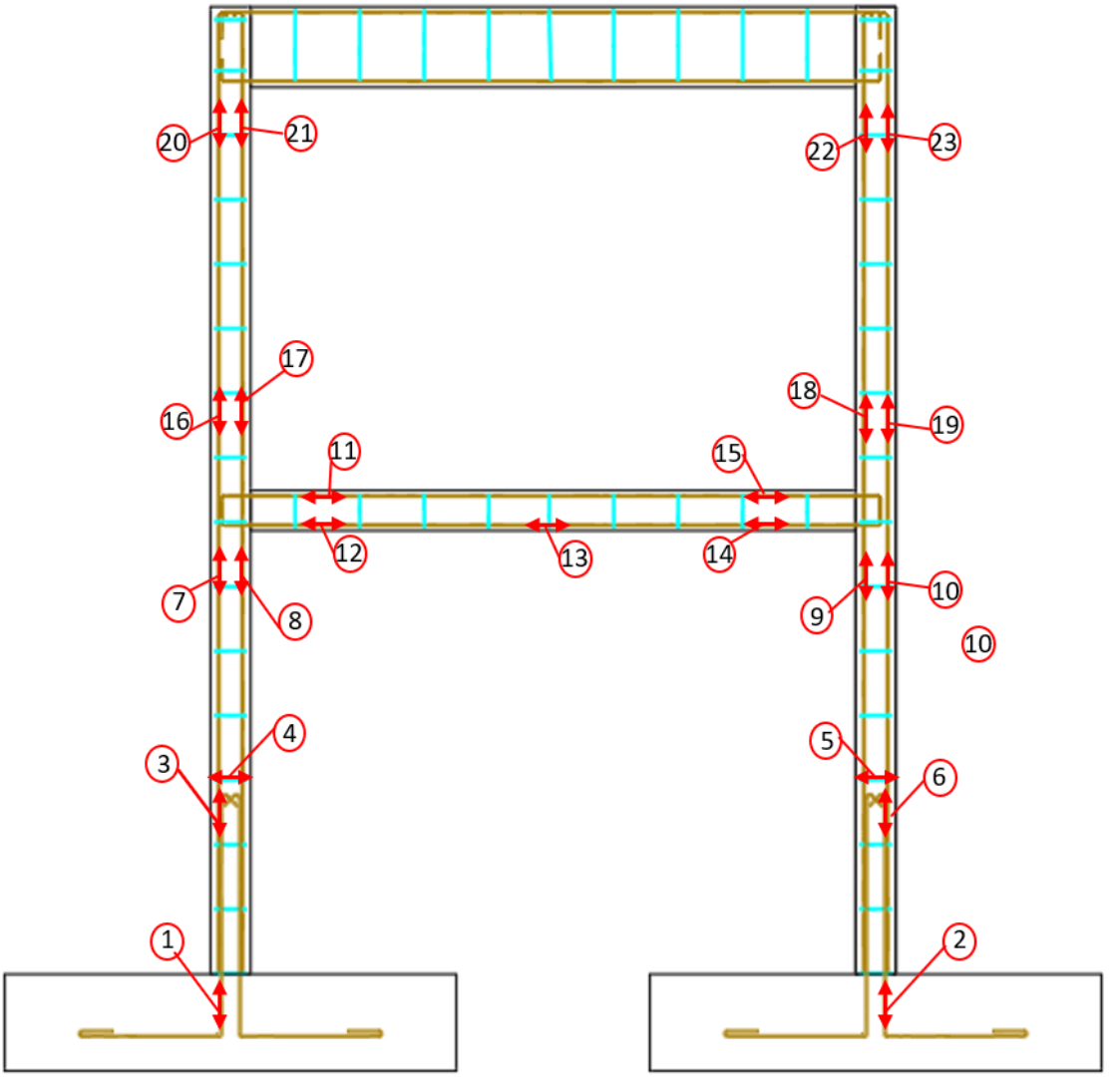

Fig. 5: Location of strain gages on frames.

of 200 Hz. The frames were hit with a small hammer at various points, and the accelerometers recorded the acceleration response history, which were explored using the frequency domain decomposition procedure to determine the natural period. Monotonic push load testing was conducted utilizing an actuator affixed to the reaction frame, with the frames and strong floor secured by bolts inserted into the footing. Displacements were measured using Keyence IL-600 laser displacement sensors (LDS), which operate based on output signal voltage and have a range of 200 mm to 1000 mm. For calibration, an object was placed at a known range, progressed by 5 cm, and the recorded data was used to calculate the calibration constant, which was found to be 20. During testing, the sensors were clamped to a fixed support. Fig. 6 shows the adopted test setup.

3. Results and discussion

This section provides the results of the research work on strengthening a typical soft-storey RC building utilizing parameters derived from numerical optimization. It includes findings from material tests, load vs. displacement analysis, ambient vibration tests, and strain gauge measurements. Additionally, comparisons of inter-storey drift ratios and displacements between the ground floor and first floor, stiffness degradation, and energy dissipation capacities are discussed. Crack propagation at significant drift levels of 0.5%, 1.0%, and 2.0% for both the soft-storey and strengthened frames are also analyzed, along with related graphs and images. The monitored findings demonstrate that the strengthening solution effectively eliminated the soft-storey effect, validating the approach obtained from numerical optimization.

3.1 Material test results

Depending on the experimental findings of the material tests, the quantities were renewed in the numerical model, and the analysis was rerun. SCC was utilized for the concrete components, including columns, beams, and slabs. Due to construction challenges related to the curved sections, a 30 mm gap was left, which was filled with high-strength mortar.

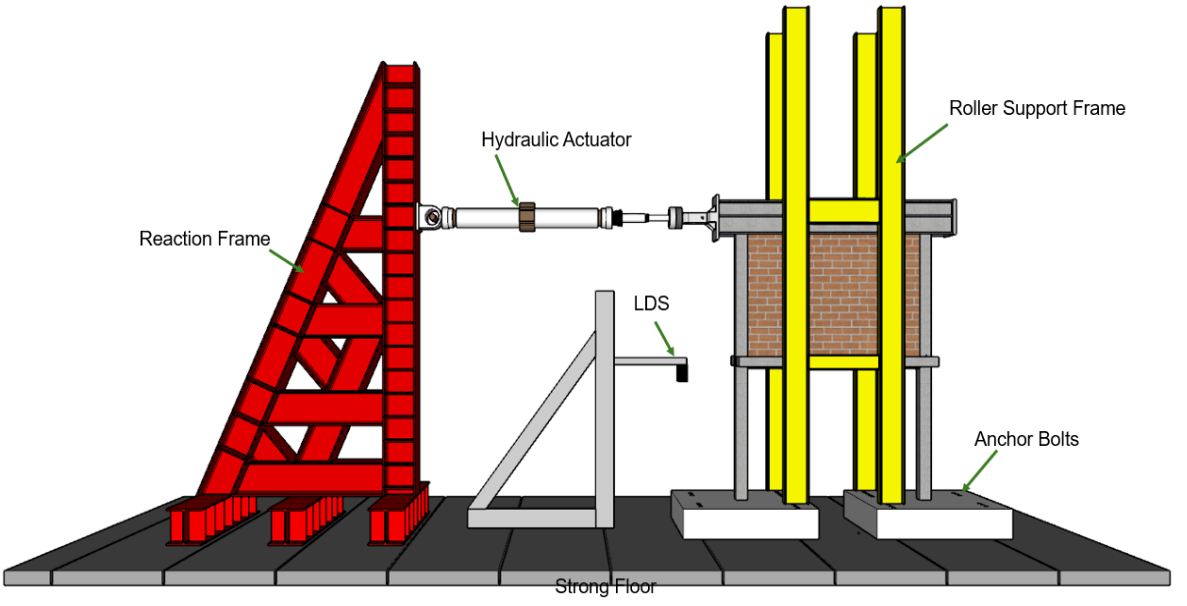

Fig. 6: Graphical representation of experimental test setup.

For each mix of 1 cubic meter, three cylindrical samples were taken and cured in water to maintain moisture. These samples were tested for compressive strength using a Universal Testing Machine (UTM) at AIT's structural lab at intervals of 7, 14, and 28 days. The average compressive strength at 28 days was found to be 22 MPa, in accordance with ASTM C39 standards.[28] Fig. S5 shows specimen failure under compression that accompanied typical concrete crushing and splitting throughout the height of specimens. Fig. 7 shows the compressive strength vs. strain results. From the graph, two distinct regions were identified: an elastic (linear) portion and a plastic (nonlinear) portion. The initial elastic segment was used to determine Young's modulus of the concrete specimens. The stiffness of the elastic segment was determined, yielding a mean elastic modulus of 20,540 MPa, with a failure strain of 0.002. These values were considered relevant and were subsequently updated in the numerical model to rerun the simulation.

To investigate the tensile capacity of the concrete specimens, the split tensile test was conducted. In this test, cylindrical samples were put in their longitudinal direction between two steel rods, and a load was applied utilizing a UTM. The failure load was logged for at least three specimens, and the tensile capacity was determined utilizing the following model using Eq. (1):

$$f_t = \frac{2P}{\pi LD} \quad (1)$$

where P is failure load, L is the length of the concrete sample and D is the diameter of the concrete sample. The average tensile capacity was determined to be 2.76 MPa and this value was utilized in the numerical analysis in its rerun.

To examine the strengths of the steel bars, three specimens of 9 mm diameter bars were tested by stretching them to the rupture point using UTM. Rebars, each with a length of 600 mm, were fitted with steel strain gauges and securely gripped in the UTM. The tests revealed a mean yield strength of 390 MPa and an average ultimate strength of 515 MPa.

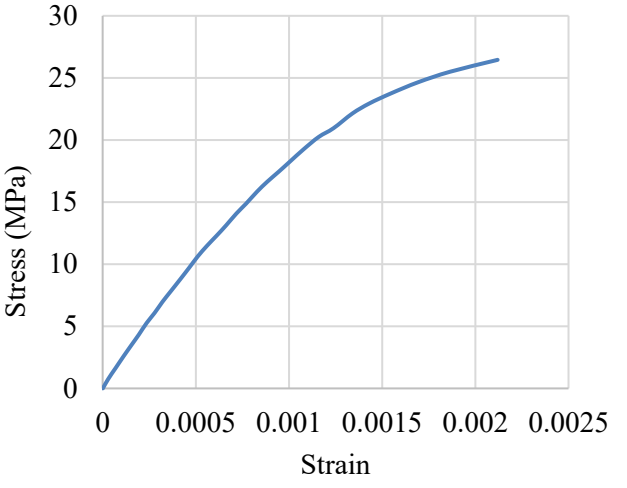

Fig. 7: Compressive strength vs strain curve of concrete.

The average brick sizes from various countries were reviewed, and based on availability and typical dimensions worldwide, the brick size selected for use was 260 mm × 120 mm × 100 mm (Dream Civil, n.d.). For this study, the bricks required to be scaled down by a factor of 2, so half-sized bricks meeting these criteria were acquired. The compressive capacity of the scaled bricks was tested.[29] and it was determined to be 5.13 MPa. A total of nine 50 mm-cube mortar specimens were prepared and tested at 3 and 28 days to assess the difference in compressive strength. The tests were conducted using UTM at AIT's Structural Engineering Laboratory. The compressive capacity of the mortar at 28 days

was determined to be 5.16 MPa. Fig. S6 shows the failure of mortar and brick specimens.

3.2 Load vs. deflection response of frames

The load-displacement graph is crucial for illustrating the peak load and deflection characteristics of both frames. The peak capacity recorded was approximately 7 kN for the soft-storey frame and 73 kN for the strengthened frame, indicating a tenfold increase in peak load capacity with the strengthening strategy. Since the strengthened frame was tested up to only 2% lateral drift, all comparative analyses of the results shall be conducted up to this 2% lateral drift limit. Pushover curves of control and strengthened frames are shown in Fig. 8.

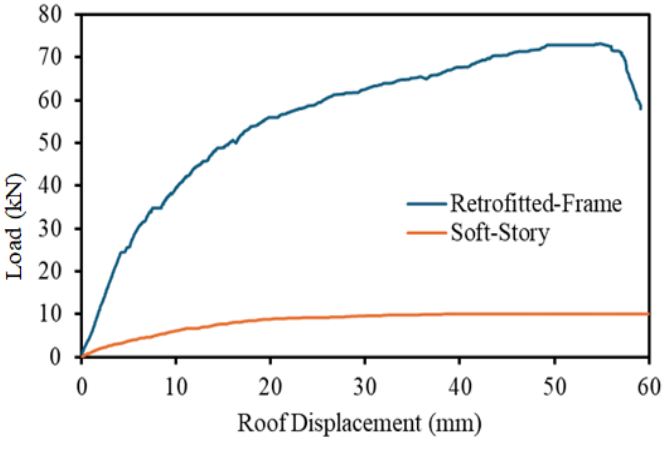

Fig. 8: Pushover curves of frames.

3.3 Dissipated energy

A frame with good ability for dissipated energy is considered effective in absorbing energy induced by seismic actions. These characteristic aids protect various structural components by reducing the input energy, allowing all critical systems to function effectively within the elastic range. Dissipated energy is assessed by determining the area under the load vs. displacement curve at each step up to the peak capacity, as shown in Fig. 9. The analysis revealed that the dissipated energy in the strengthened frame is five times higher than in the soft-storey frame. This indicates that the strengthened frame is significantly stronger and capable of absorbing much more energy from earthquakes compared to the soft-storey frame.

3.4 Inter-storey drift and displacement results

The comparison of inter-storey drift ratios and displacements is crucial for evaluating the sway movement of both the soft-storey frame and the strengthened frame, which aims to mitigate the soft-storey effect. Findings were graphically demonstrated at significant drift ratios of 0.5%, 1%, and 2%, as shown in Fig. 10. It was observed that the soft-storey frame experienced substantial displacements at the ground floor compared to the first floor, due to the ground floor's notably lower stiffness. However, this soft-storey impact was effectively eradicated in the strengthened frame, demonstrating improved performance and reduced displacement. Fig. 11 shows a comparison of inter-storey drift ratio of control and strengthened frames. It is noted that the strengthened frame demonstrated significantly lower inter-storey drift at each drift ratio than the control frame.

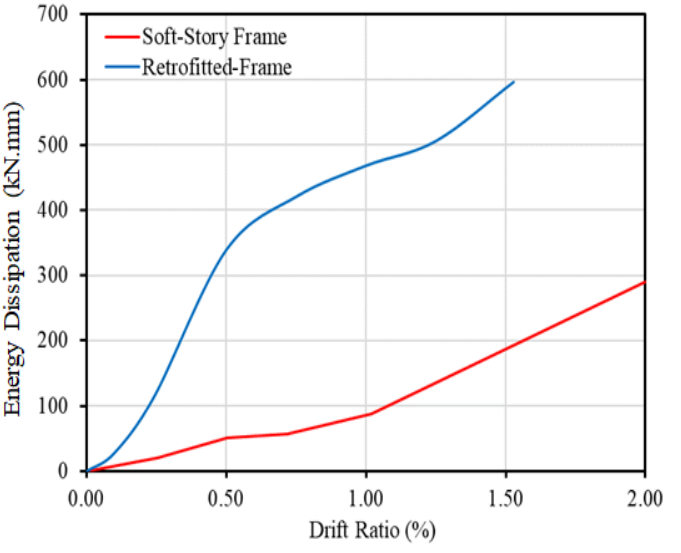

Fig. 9: Evolution of energy dissipation of frames with respect to drift ratio.

3.5 Stiffness degradation results

Stiffness degradation is a crucial factor in assessing a building's seismic behavior, as it reflects the accumulated damage from seismic actions. Stiffness was determined by dividing the force by the displacement at each step. The analysis revealed that the stiffness of the strengthened frame is approximately 10 times greater than that of the soft-storey frame, as shown in Fig. 12. This significant increase in stiffness is attributed to the added curves, which are connected to both the columns and beams on the ground floor, enhancing the overall structural integrity of the strengthened frame.

3.6 Comparison of natural frequency of frames

The natural frequency provides insight into the dynamic behavior and stiffness of the frames. For the soft-storey frame, the calculated natural frequency was nearly identical to the numerical value, with a calculated frequency of 10.85 Hz compared to a numerical value of 10.45 Hz from the AEM analysis. This numerical value accounts for the added floor weight and the weight of the jack. In contrast, the measured natural frequency for the strengthened frame was lower than the numerical prediction. The measured frequency was 25.62 Hz, whereas the numerical value from the AEM analysis was 30.55 Hz, as shown in Fig. 13. This difference may be ascribed to factors such as construction variations and the bonding between old and new concrete.

3.7 Crack propagation patterns

During experiments, crack patterns were inspected and marked to correlate with the applied load. After the experiment,

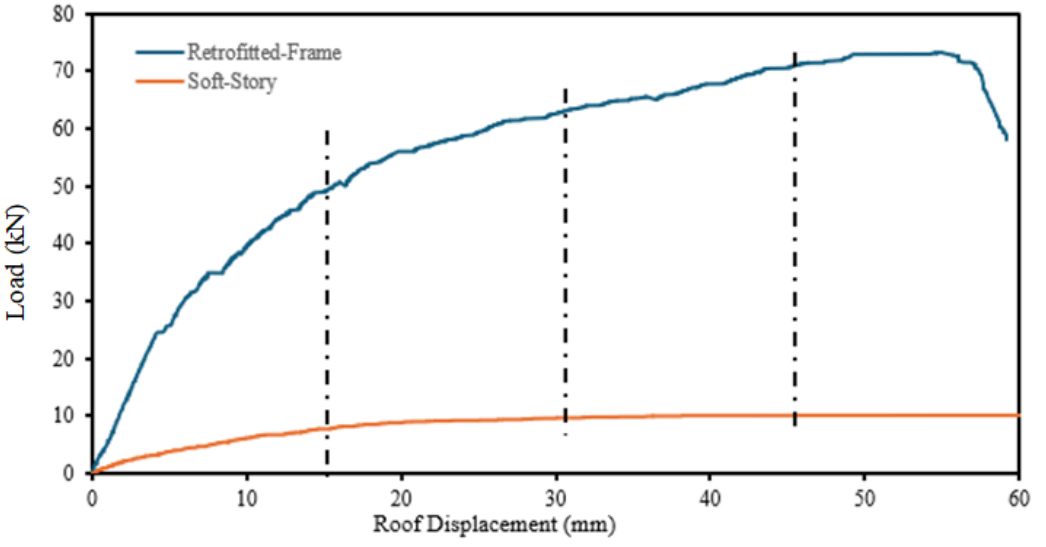

Fig. 10: Inter-storey drift and displacements of control and strengthened frames.

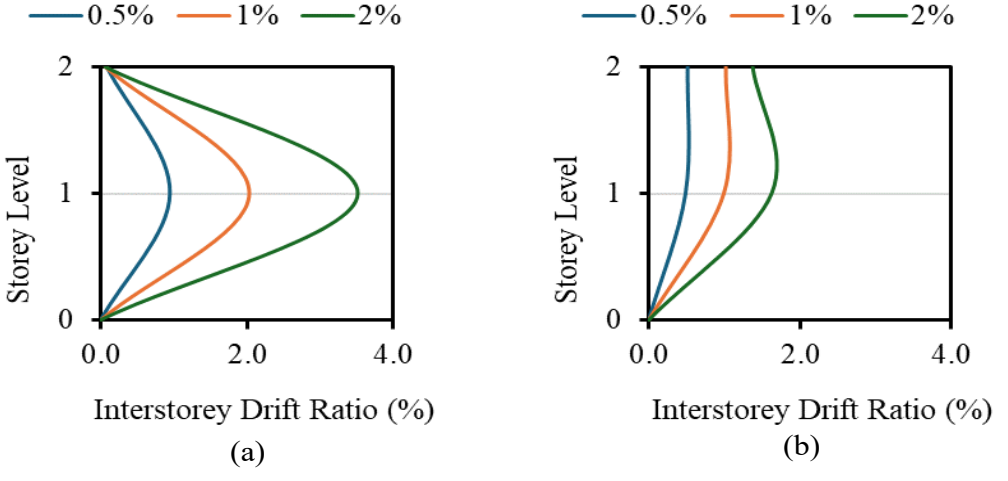

Fig. 11: Inter-storey drift at various drifts ratios for (a) control and (b) strengthened frame.

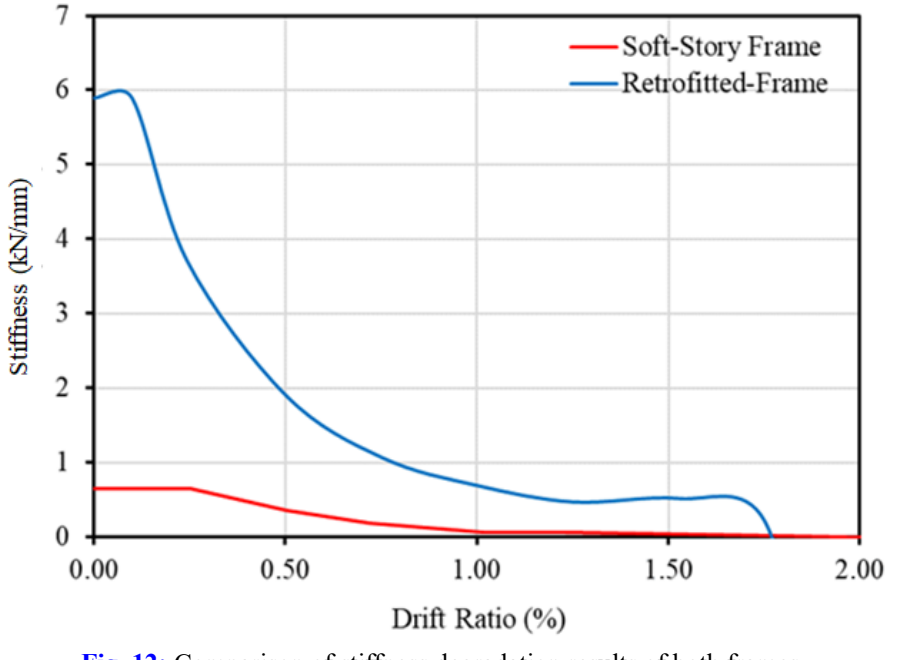

Fig. 12: Comparison of stiffness degradation results of both frames.

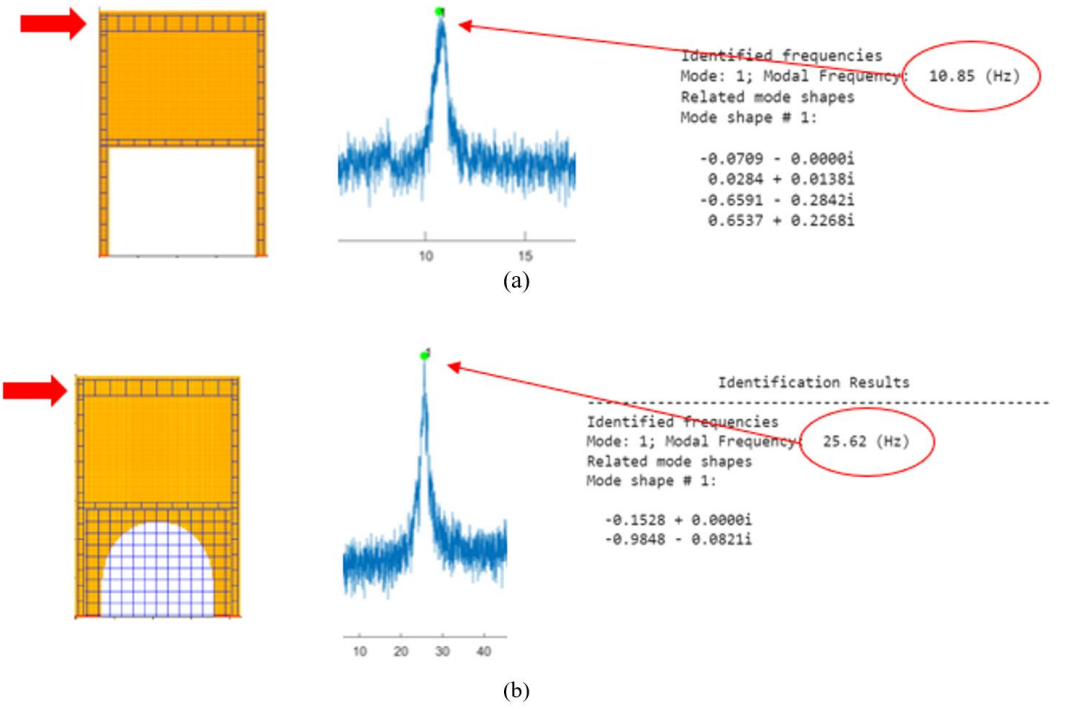

Fig. 13: Frequency decomposition of vibration response of (a) control and (b) strengthened frame.

these patterns were outlined and recorded. As anticipated for soft-storey buildings, ground floor columns of the soft-storey frame demonstrated the first cracks. With increasing displacements, crack propagation was concentrated on the ground floor columns. At 0.50% drift, flexural cracks were observed at both the top and bottom of the ground floor column on the loading side, while the opposite side showed some inner-side cracks. This observation indicates that soft-storey buildings can exhibit significant deformations and crack accumulation predominantly at the open floor level. Specifically, the bottom of the ground floor column on the loading side experienced tension, resulting in noticeable flexural cracks, as shown in Fig. 14(a). In the strengthened frame, at 0.50% drift, flexural cracks were observed at the top of the first-floor column on the loading side, along with a separation crack between the mortar and the curved portion, as shown in Fig. 14(b). These cracks may be ascribed to the differing properties of the materials used, which could affect their interaction and bond strength.

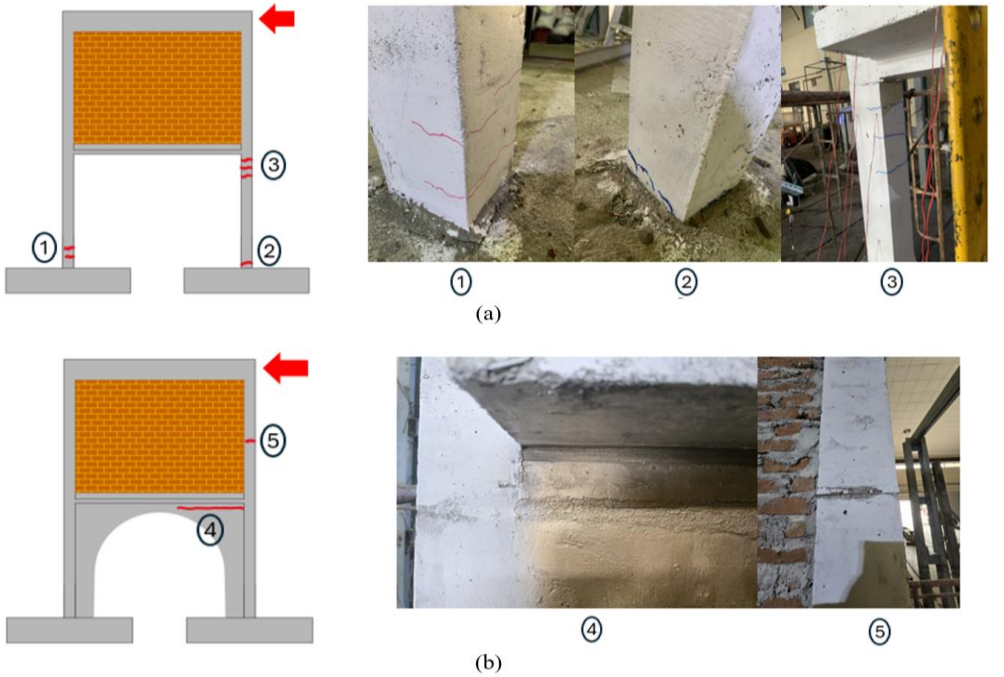

Fig. 14: Comparison of crack patterns at 0.5% drift ratio in (a) control and (b) strengthened frame.

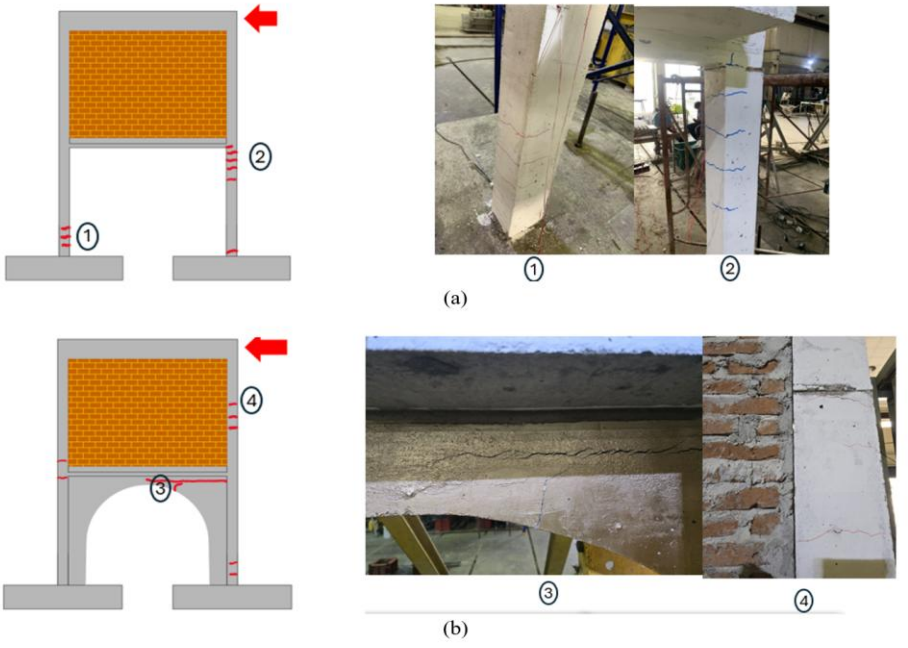

Fig. 15: Comparison of crack patterns at 1.0% drift ratio in (a) control and (b) strengthened frame.

At 1.0% drift, the flexural cracks at both the top and bottom of the ground floor column on the loading side of the soft-storey frame became more pronounced, with additional cracks developing on the inner side. In the strengthened frame, at the same drift level, flexural cracks appeared at both the ground and first-floor columns on the loading side, with some additional cracks developing near the floor on the opposite side. The separation crack between the mortar and the curved portion also widened significantly, which may be attributed to the differing properties of the materials used. The comparison of cracks at 1.0% drift ratio is illustrated in Fig. 15.

At 2.0% drift, the flexural cracks at both the top and bottom of the ground floor column on the loading side of the soft-storey frame expanded further, with additional cracks appearing on the inner side. All cracks were concentrated on the ground floor columns. In the strengthened frame, at the same drift level, additional flexural cracks were observed at both the ground and first-floor columns on the loading side, with more cracks developing near the floor on the opposite side. The separation crack between the mortar and the curved portion continued to widen, likely due to the differing material properties. Additionally, a diagonal crack developed in the brick wall. The comparison of cracks at 2.0% drift ratio is illustrated in Fig. 16.

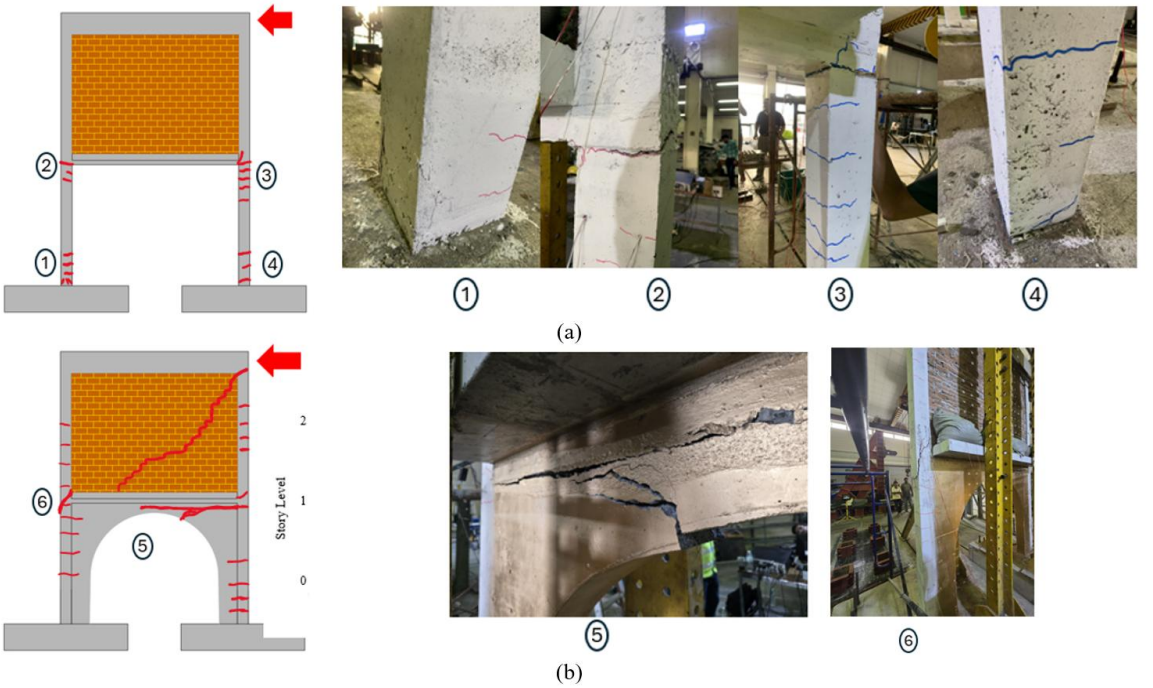

Fig. 16: Comparison of crack patterns at 2.0% drift ratio in (a) control and (b) strengthened frame.

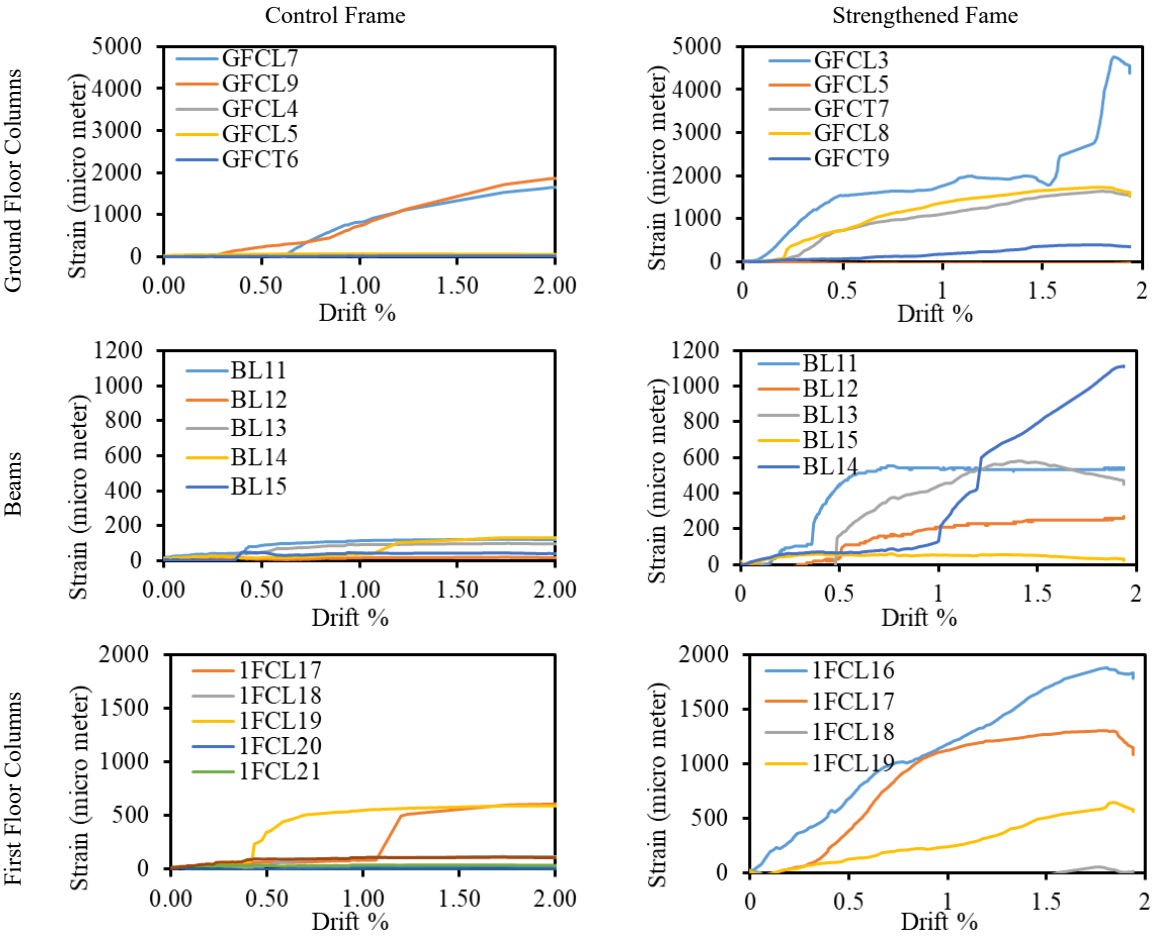

Fig. 17: Comparison of steel bar strains in control and strengthened frame.

3.8 Strain gage results

Given the yield strength of 390 MPa and the elastic modulus of the rebar at 210 GPa, the calculated yield strain was 1910 micro strain. In the soft-storey frame, the strain in the rebars of the ground floor columns was noted to surpass this yield strain limit. In the strengthened frame, the rebars in both the ground and first-floor columns, as well as in the beams, also surpassed the strain limit. Fig. 17 shows the comparison of longitudinal steel bar strains of control and strengthened frames. It is noted that steel bar in columns of ground floor and first floor, and beams of strengthened frame demonstrated greater strains than the control frame. This reflects the greater flexural potential of the strengthened frame in comparison to the control frame.

4. Conclusion

This research aims to experimentally validate and establish guidelines for an optimized RC infill wall strengthening strategy, focusing on local availability, response, price, usability, and difficulty. The study pursued two key objectives: (1) analyzing soft-storey frames using AEM-based numerical optimization to develop an effective strengthening solution, and (2) experimentally verifying the performance of the optimized RC infill wall in strengthening soft-storey buildings. Based on experimental findings, the following conclusions may be drawn.

The strengthening solution significantly enhanced the structural performance, as evidenced by the maximum peak load recorded at approximately 7 kN for the soft-storey frame compared to 73 kN for the strengthened frame, demonstrating a tenfold increase in peak load capacity. The analysis indicated that the strengthened frame dissipated energy at a level five times higher than that of the soft-storey frame, underscoring the superior strength and seismic energy absorption capacity of the strengthened frame.

The soft-storey frame exhibited substantial displacements at the ground floor relative to the first floor, attributed to the significantly lower stiffness of the ground floor, resulting in a pronounced soft-storey effect. However, this effect was effectively mitigated in the strengthened frame, which demonstrated improved performance characterized by reduced overall displacements. Additionally, the strengthened frame showed significantly lower inter-storey drift at each drift ratio compared to the control frame, highlighting its enhanced stability and stiffness.

The analysis revealed that the stiffness of the strengthened frame is approximately ten times higher than that of the soft-storey frame. This substantial increase in stiffness is primarily attributed to the addition of curves connected to both the columns and beams on the ground floor, which significantly enhanced the overall structural integrity of the strengthened frame.

For the soft-storey frame, the measured natural frequency closely matched the numerical prediction, with a measured frequency of 10.85 Hz compared to a numerical value of 10.45 Hz obtained from the AEM analysis, which included the effects of the added floor weight and the weight of the jack. In contrast, the strengthened frame exhibited a measured natural frequency of 25.62 Hz, which was lower than the numerical prediction of 30.55 Hz. This discrepancy may be ascribed to factors such as construction variations and the bonding quality between the existing and newly added concrete.

Acknowledgement

This study Received Research Funding from Srinakharinwirot University, Thailand Income for Fiscal Year 2024 (Contract Number 492/2567). Thanks, are also extended to Asian Institute of Technology (AIT), Thailand for supporting test facilities.

Conflict of Interest

There is no conflict of interest.

Supporting Information

Applicable.

References

[1] ASCE/SEI 41-17, Seismic Evaluation and Retrofit of Existing Buildings, American Society of Civil Engineers, 2017, doi: 10.1061/9780784414859.

[2] I. Ul Haq, A. Elahi, A. Nawaz, S. Aamir Qadeer Shah, K. Ali, Mechanical and durability performance of concrete mixtures incorporating bentonite, silica fume, and polypropylene fibers, *Construction and Building Materials*, 2022, **345**, 128223, doi: 10.1016/j.conbuildmat.2022.128223.

[3] K. Rodsin, P. Joyklad, Q. Hussain, H. Mohamad, A. Buatik, M. Zhou, K. Chaiyasarn, A. Nawaz, T. Mehmood, E. Amr, Behavior of steel clamp confined brick aggregate concrete circular columns subjected to axial compression, *Case Studies in Construction Materials*, 2022, **16**, e00815, doi: 10.1016/j.cscm.2021.e00815.

[4] S. Farhan Mushtaq, A. Ali, R. A. Khushnood, R. F. Tufail, A. Majdi, A. Nawaz, S. Durdyev, D. D. Burduhos Nergis, J. Ahmad, Effect of bentonite as partial replacement of cement on residual properties of concrete exposed to elevated temperatures, *Sustainability*, 2022, **14**, 11580, doi: 10.3390/su141811580.

[5] I. Ahmad Rana, S. Khaled, A. Jamshed, A. Nawaz, Social protection in disaster risk reduction and climate change adaptation: A bibliometric and thematic review, *Journal of Integrative Environmental Sciences*, 2022, **19**, 65-83, doi: 10.1080/1943815x.2022.2108458.

[6] H. S. A. Varum, Seismic assessment, strengthening and repair of existing buildings, Masters Thesis, Universidade de Aveiro, 2003.

[7] S. Ahmad, A. Shah, A. Nawaz, K. Salimullah, Shear strengthening of corbels with carbon fibre reinforced polymers (CFRP), *Materiales de Construcción*, 2010, **60**, 79-97, doi: 10.3989/mc.2010.50009.

[8] X. Romão, A. A. Costa, E. Paupério, H. Rodrigues, R. Vicente, H. Varum, A. Costa, Field observations and interpretation of the structural performance of constructions after the 11 May 2011 Lorca earthquake, *Engineering Failure Analysis*, 2013, **34**, 670-692, doi: 10.1016/j.engfailanal.2013.01.040.

[9] P. Joyklad, A. Nawaz, Q. Hussain, Effect of fired clay brick aggregates on mechanical properties of concrete, *Suranaree Journal of Science and Technology*, 2018, **25**, 349-362.

[10] M. Usman, M. Yaqub, M. Auzair, W. Khaliq, M. Noman, A. Afaq, Restorability of strength and stiffness of fire damaged concrete using various composite confinement techniques, *Construction and Building Materials*, 2021, **272**, 121984, doi: 10.1016/j.conbuildmat.2020.121984.

[11] S. Matiyas, N. Workeluel, T. Mohanty, P. Saha, Review of different analysis and strengthening techniques of soft story buildings, *Materials Today: Proceedings*, 2023, doi: 10.1016/j.matpr.2023.04.231.

[12] J. Wilson, N. Lam, K. Rodsin, Collapse modelling of soft-storey buildings, *Australian Journal of Structural Engineering*, 2009, **10**, 11-23, doi: 10.1080/13287982.2009.11465029.

[13] P. D. Gkournelos, T. C. Triantafillou, D. A. Bournas, Seismic upgrading of existing reinforced concrete buildings: A state-of-the-art review, *Engineering Structures*, 2021, **240**, 112273, doi: 10.1016/j.engstruct.2021.112273.

[14] A. Husnain, I. A. Qazi, W. Khaliq, M. Arshad, Immobilization in cement mortar of chromium removed from water using titania nanoparticles, *Journal of Environmental Management*, 2016, **172**, 10-17, doi: 10.1016/j.jenvman.2016.02.026.

[15] P. D. Gkournelos, T. C. Triantafillou, D. A. Bournas, Seismic upgrading of existing reinforced concrete buildings: A state-of-the-art review, *Engineering Structures*, 2021, **240**, 112273, doi: 10.1016/j.engstruct.2021.112273.

[16] J. W. Bai, M. A. Center, M. B. Hueste, Seismic retrofit for reinforced concrete building structures, *Mid-America Earthquake Center*, CM-4, 2003.

[17] G. E. Thermou, A. S. Elnashai, Seismic retrofit schemes for RC structures and local-global consequences, *Progress in Structural Engineering and Materials*, 2006, **8**, 1-15, doi: 10.1002/pse.208.

[18] P. P. Chandurkar, P. S. Pajgade, Seismic Analysis of RCC Building with and Without Shear Wall, *International Journal of Modern Engineering Research*, 2013, **3**, 1805-1820.

[19] S. Pujol, A. Benavent-Climent, M. E. Rodriguez, J. P. Smith-Pardo, Masonry infill walls: an effective alternative for seismic strengthening of low-rise reinforced concrete building structures, *14th World Conference on Earthquake Engineering*, Tokyo, Japan, 2008, 12-17.
[20] A. Ghobarah, H. Abou Elfath, Rehabilitation of a reinforced concrete frame using eccentric steel bracing, *Engineering Structures*, 2001, **23**, 745-755, doi: 10.1016/S0141-0296(00)00100-0.
[21] G. Oliveto, M. Marletta, Seismic retrofitting of reinforced concrete buildings using traditional and innovative techniques, *ISET Journal of Earthquake Technology*, 2005, **42**, 21-46, doi: 10.63898/xrsm2168.
[22] D. D. Ahiwale, R. R Khartode, Evaluation seismic response for soft storey building retrofitted with infill, steel bracing and shear wall, *Journal of Structural Technology*, 2020, **5**, 1-13, doi: 10.46610/jost.2020.v05i02.001.
[23] K. Timsina, C. G. Krishna, K. Meguro, Sociotechnical evaluation of the soft story problem in reinforced concrete frame buildings in Nepal, *Journal of Performance of Constructed Facilities*, 2021, **35**, 04021019, doi: 10.1061/(asce)cf.1943-5509.0001582
[24] S. S. Rao, Engineering Optimization Theory and Practice, Wiley, 2019, ISBN: 101119454719.
[25] A. Eraky, S. A. Mustafa, M. Badawy, Structural analysis using Applied Element Method: a review, *The Egyptian International Journal of Engineering Sciences and Technology*, 2021, **34**, 16-27, doi:10.21608/eijest.2021.56786.1043.
[26] K. Timsina, C. K. Gadagamma, M. Numada, K. Meguro, Development of a numerical optimization framework for solving soft-storey problem in reinforced concrete frame buildings, *Seisan Kenkyu*, 2019, **71**, 813-823, doi: 10.11188/seisankenkyu.71.813.
[27] F. A. Noor, L. F. Boswell, Small scale modelling of concrete structures, CRC Press, 1992, 357, ISBN: 9780429182334.
[28] ASTM C39/C39M-21, Standard Test Method for Compressive Strength of Cylindrical Concrete Specimens, ASTM International, West Conshohocken, PE, USA, 2021.
[29] ASTM C1314-23a, Standard Test Method for Compressive Strength of Masonry Prisms, ASTM International, West Conshohocken, PE, USA, 2023.